International Journal of Minerals, Metallurgy and Materials
Volume 26, Number 9, September 2019, Page 1177
https://doi.org/10.1007/s12613-019-1829-2

Novelty phase synthesis mechanism and morphology in resin-bonded Al–Al_2O_3–TiO_2 composites at high temperatures under flowing N_2

Yang Sun[1)], *Yong Li*[1)], *Li-xin Zhang*[2)], *Shi-ming Li*[3)], *Ming-wei Yan*[1)], *and Jia-lin Sun*[1)]

1) School of Materials Science and Engineering, University of Science and Technology Beijing, Beijing 100083, China
2) Sinosteel Refractory Co. Ltd., Henan 471039, China
3) Beijing Cisri-nmt Environmental Science and Technology Co. Ltd., Beijing 100083, China
(Received: 15 December 2018; revised: 12 March 2019; accepted: 17 March 2019)

Abstract: An Al–AlN core–shell structure is beneficial to the performance of Al–Al_2O_3 composites. In this paper, the phase evolution and microstructure of Al–Al_2O_3–TiO_2 composites at high temperatures in flowing N_2 were investigated after the Al–AlN core–shell structure was created at 853 K for 8 h. The results show that TiO_2 can convert Al into Al_3Ti (~1685 K), which reduces the content of metal Al and rearranges the structure of the composite. Under N_2 conditions, Al_3Ti is further transformed into a novelty non-oxide phase, TiCN. The transformation process can be expressed as follows: Al_3Ti reacts with C and other carbides (Al_4C_3 and Al_4O_4C) to form TiC_x ($x < 1$). As the firing temperature increases, Al_3Ti transforms into a liquid phase and produces Ti(g) and TiO(g). Finally, Ti(g) and TiO(g) are nitrided and solid-dissolved into the TiC_x crystals to form a TiCN solid solution.

Keywords: aluminum; titanium oxide; alloys; titanium carbonitride

1. Introduction

In the 1970 s, Japanese researchers introduced graphite into magnesia and prepared magnesia–carbon refractories, which prolonged the service life of refractories for EAF (electric arc furnace) and BOF (basic oxygen furnace) tenfold compared with the original oxide refractories [1]. Carbon-containing refractories can generate a series of non-oxide-reinforced phases during the firing process via carbothermal reduction and nitridation processes [2], and carbon itself has good thermal conductivity and is not easily wettable by molten Fe. Thus, carbon composite refractories exhibit good thermal shock stability, excellent resistance to slag erosion, and a low coefficient of thermal expansion. However, carbon easily dissolves into molten steel, resulting in carburization of the steel, which is inconsistent with the carbon content standards for molten Fe during steelmaking [3]. Compared with carbon composite refractories, oxide–non-oxide composites have superior oxidation resistance and high-temperature strength and can be used without firing (prepared by direct nitridation with the use of metal–oxide composites [4]). Obviously, the use of non-oxides can reduce the carbon content in the refractory, making the refractory environmentally friendly.

When resin-bound Al–Al_2O_3 is fired under a N_2 atmosphere, non-oxide bonding phases such as Al_4C_3, Al_4O_4C, and Al_2OC_{ss} [5–7] are formed in the material as the temperature increases. Al_4C_3 is easily hydrated [8]. Al_4O_4C and Al_2OC_{ss} are incongruent-melting compounds in the Al_4C_3–Al_2O_3 binary system, with decomposition temperatures of approximately 2143 K and 2263 K, respectively; they also exhibit high thermal conductivity, good thermal shock resistance, a low wetting angle to liquid steel, better hydration resistance than Al_4C_3, and much better oxidation resistance than graphite and carbon black [9–16]. However, Al_2OC_{ss} can be stable at high temperatures (>1988 K [11,15]) and in the coexistence of AlN [17]. Although Al_4O_4C has a low formation temperature (approximately 1473 K [5]), it is unstable under ultralow oxygen partial pressures [8,18–20].

TiO_2 cannot exist stably when coexisting with C or metallic Al and is further reduced to Al–Ti alloy or TiC [21–24]. Compared with Al, Al–Ti alloys have higher melting points,

Corresponding author: Yong Li E-mail: lirefractory@vip.sina.com

and TiC is characterized by a high melting point, high hardness, and good oxidation resistance [25–26]. In the present study, Al powder, rutile TiO_2 powder, and brown fused corundum were used as raw materials, thermosetting phenolic resin was used as a binder, the phase evolution and microstructure of Al–Al_2O_3 and Al–Al_2O_3–TiO_2 composites at high temperatures under flowing N_2 were studied, and the effect of TiO_2 on Al–Al_2O_3 materials was explored.

2. Theoretical analysis

The melting point of Al is 933 K, and its liquid viscosity (0.104 Pa·s) is close to that of water at 293 K (0.10 Pa·s). Liquid Al, with a low viscosity, can hinder both the nitridation reaction and the carbothermal reaction, further contributing to the inhomogeneity of the reaction product and weakening the properties of the end product at high temperatures. A layer of AlN shell can be formed on the surface of metallic Al particles when the material is maintained at 853 K under N_2 conditions [27]. The construction of the Al–AlN core–shell structure can increase the temperature of metal Al participating in the reaction. However, the formation reaction of AlN is kinetically difficult at 853 K, and the metallic Al fluid still exists in the material.

When Al and TiO_2 are simultaneously present in the system, TiO_2 cannot be stably present. The following reaction will occur:

$$(3x+4)\,Al(l)+3TiO_2(s)=2Al_2O_3(s)+3Al_xTi(s) \quad (1)$$

The Al–Ti binary phase diagram (Fig. 1) shows that the Al_xTi generated in Eq. (1) includes $AlTi_3$, Al_2Ti, AlTi, and Al_3Ti. The expressions for the Gibbs free energy of these substances as a function of temperature are shown in Table 1 [28], and the corresponding relationship between the Gibbs free energy and temperature is shown in Fig. 2. As evident in Fig. 2, the Gibbs free energies of the four Al–Ti binary compounds are negative. Although the Gibbs free energy of Al_2Ti is lower than that of Al_3Ti, studies have shown that Al_3Ti is the main product of the Al–Ti binary system [29]. Al_3Ti is the main product because it is a type-I compound that can be formed by direct reaction, whereas Al_2Ti is a type-II compound whose formation requires an AlTi phase and a series of solid–solid or solid–liquid reactions [30]. Thus, the reaction that can occur between Al and TiO_2 is

$$13Al(l)+3TiO_2(s)=2Al_2O_3(s)+3Al_3Ti(s) \quad (2)$$

The metal Al in Al–Al_2O_3–C systems has been reported to change according to the process Al → Al_4C_3 → Al_4O_4C → $(Al_2OC)_x(AlN)_{1-x}$ under N_2 conditions [6–7]. When Al_3Ti is introduced to form an Al–Al_3Ti–C system, the following reactions will occur in the material [31]:

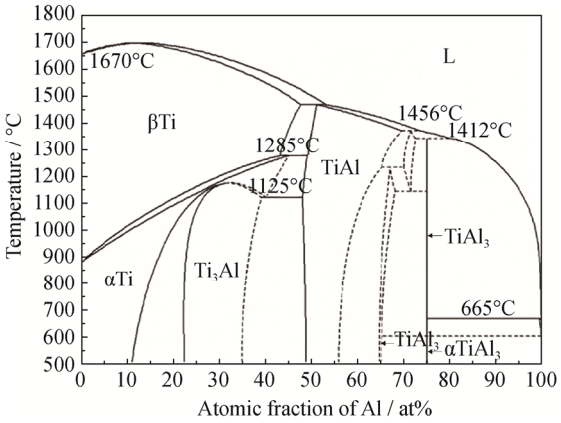

Fig. 1. Al–Ti binary phase diagram.

Table 1. Expression of the Gibbs free energy of Ti–Al-based intermetallic compounds with temperature [28]

Compound	ΔG / (J·mol^{-1})
Ti_3Al	$-29633.6 + 6.708T$
TiAl	$-37445.1 + 16.974T$
Al_2Ti	$-43858.4 + 11.021T$
Al_3Ti	$-40349.6 + 10.365T$

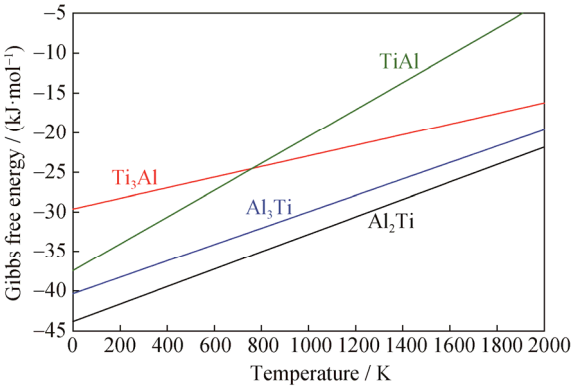

Fig. 2. Relationship between the Gibbs free energy and the temperature of Ti–Al intermetallic compounds.

$$4\,Al(l)+3\,C(s)=Al_4C_3(s) \quad (3)$$

$$3\,Al_3Ti(s)+Al_4C_3(s)=3\,TiC(s)+13\,Al(l) \quad (4)$$

$(Al_2OC)_x(AlN)_{1-x}$ is a high-temperature phase that can exist stably only at temperatures above 1988 K [11,15] and is therefore not considered. The reaction between Al_3Ti and Al_4O_4C can be expressed as

$$3\,Al_3Ti(s,l)+3\,Al_4O_4C(s)=3\,TiC(s)+13\,Al(l)+4\,Al_2O_3(s) \quad (5)$$

Eqs. (4) and (5) can spontaneously occur when the temperature is greater than 994 K and 1132 K, respectively (thermodynamic data from the NIST-JANAF thermochemical tables [32] and the Ref. [12]). (Unless otherwise stated, the thermodynamic data herein are derived from the NIST-JANAF thermochemical tables [32].) Therefore, the most thermodynamically stable carbon-containing compound in the

Al–Ti–O–C system is TiC. Al_4C_3, Al_4O_4C, etc., as intermediates, are eventually consumed by the reaction to form TiC.

The nitridation reaction of the metal Al can release a large amount of heat ($\Delta H_{Al(g)+0.5N_2(g)=AlN(s)} = -655.64448 + 0.01244T$, $kJ \cdot mol^{-1}$). Under a high-purity N_2 atmosphere (N_2 content 99.999vol%), Eqs. (4) and (5) become Eqs. (6) and (7), where Al is converted into AlN. The Gibbs free energies of Eqs. (6) and (7) at 1773 K can reach −1760 kJ and −1727 kJ, whereas those of Eqs. (4) and (5) are only −187 kJ and −153 kJ, respectively.

$$3Al_3Ti(s) + Al_4C_3(s) + 6.5N_2(g) = 3TiC(s) + 13AlN(s) \quad (6)$$

$$3Al_3Ti(s,l) + 3Al_4O_4C(s) + 6.5N_2(g) = 3TiC(s) + 13AlN(s) + 4Al_2O_3(s) \quad (7)$$

Therefore, when TiO_2 is added to the resin-bonded Al–Al_2O_3 material and sintered under flowing N_2, molten metal Al can be converted into a high-melting-point alloy phase, Al_3Ti, thereby reducing the amount of liquid in the material. Furthermore, Al_3Ti can fix the resin residual carbon in the material and convert it into a non-oxide reinforcing phase: TiC. According to Eq. (2), the ratio of the raw materials was determined to be Al: TiO_2: C = 13:3:3 (mol%).

3. Experimental process

Raw materials were meticulously weighed and mixed in the proportions specified in Table 2. Brown fused corundum ($w(Al_2O_3) \geq 95\%$), rutile powder ($w(TiO_2) \geq 99.4\%$), and metal Al powder ($w(Al) \geq 99.3\%$) were used as the raw materials, with resin as the binding agent. After being mixed for 30 min, the aforementioned raw materials were uniaxially pressed under a pressure of 300 MPa to obtain a specimen with dimensions of 40 mm × 40 mm × 120 mm. The specimen was dried at 473 K for 24 h. Afterwards, the specimen was placed in a graphite crucible and heated according to the following temperature program: the temperature was increased from room temperature to 853 K at a rate of 10 K/min; maintained at 853 K for 8 h; increased from 853 K to 1273 K at a rate of 10 K/min; increased from 1273 K to 1573 K/1773 K at a rate of 5 K/min; and maintained at 1573 K/1773 K for 3 h. The entire experiment was performed under a flow of high-purity N_2 gas (0.101 MPa, N_2 content 99.999vol%). The samples calcined at 1573 K and 1773 K were labeled as T0-1573, T1-1573, T0-1773, and T1-1773, respectively.

Table 2. Proportions of raw materials used in this work wt%

Specimen number	Brown fused corundum				Rutile powder (TiO_2, ≤44 μm)	Aluminum powder (≤75 μm)
	5–3 mm	3–1 mm	≤1 mm	≤75 μm		
T0	10	40	15	20	—	15
T1	10	40	15	10	10	15

Note: Extra 3wt% thermosetting phenolic resin was added as the bonding agent.

4. Results and discussion

4.1. Analysis of the phase and microstructure of the specimen heated at 1573 K

Fig. 3 shows the XRD patterns of T0-1573 and T1-1573. As evident from the figure, TiC, Al_3Ti, AlN, Al_4O_4C, and Al_4C_3 were generated in T1-1573. In comparison, the diffraction peaks of Al_4O_4C and Al_4C_3 are more intense in the pattern of T0-1573.

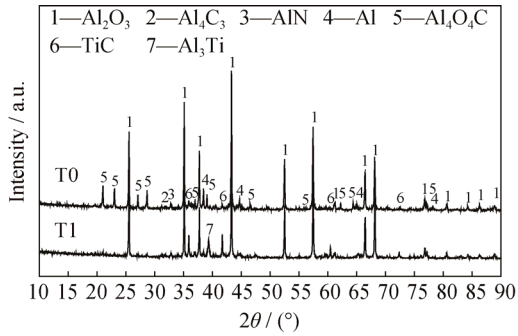

Fig. 3. XRD patterns of the specimens after sintering at 1573 K for 3 h.

Fig. 4 shows SEM images of T0-1573. The structure of T0-1573 is loose, and the pores are interpenetrating. Fine particles such as Al_4C_3, Al_4O_4C, and AlN are formed because of the flow mass transfer of metallic Al. The flow of metal Al leaves a number of regular circular holes in the matrix.

Fig. 5 shows SEM images of T1-1573. The material matrix in the images is compact. Table 3 shows the results of the EDS analysis conducted at different selected areas in Fig. 5(b), where the Al_3Ti alloy is labeled location 1, in which a small amount of solid solution of Si originates from the impurities in brown corundum. The bright-white particles in the alloy are TiC, and the dark-gray particles are Al_2O_3. These results demonstrate that TiO_2 is capable of absorbing metal Al (~933 K) and converting it into a high-melting-point Al_3Ti (~1685 K) at high temperatures. The reaction process causes the rearrangement of the structure of the material, and the presence of rigid particles such as TiC and Al_2O_3 in the alloy phase can further increase its viscosity and avoid component inhomogeneity of the material at high temperatures.

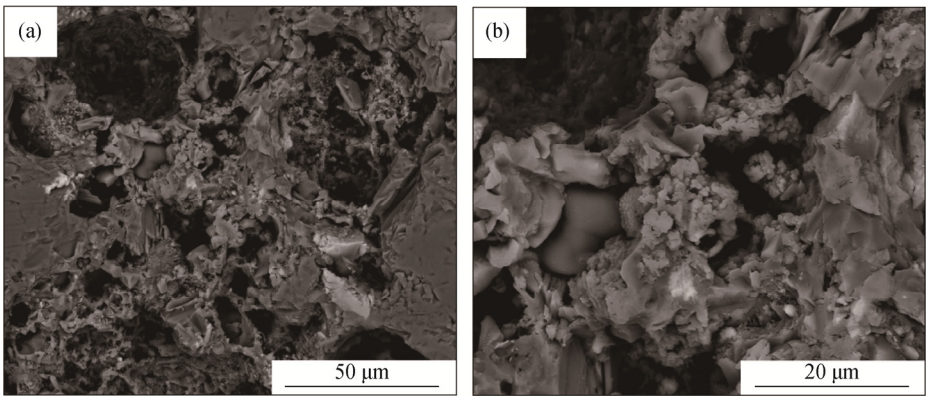

Fig. 4. SEM images of T0-1573: (a) macro image; (b) partially magnified image.

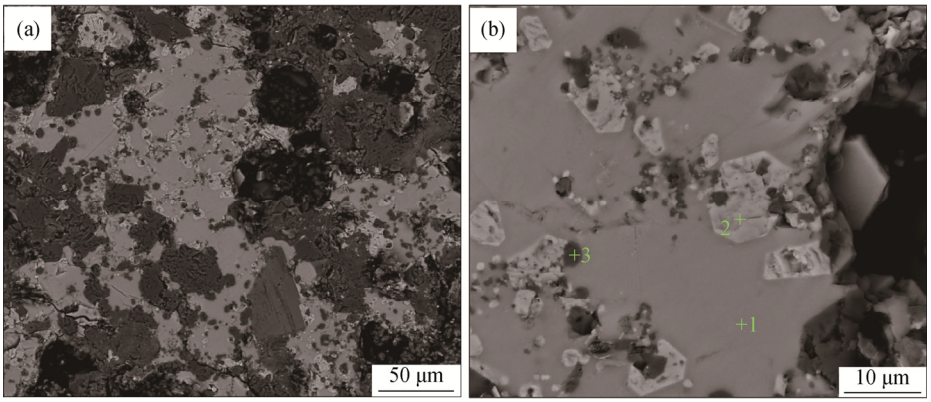

Fig. 5. SEM images of T1-1573: (a) macro image; (b) partially magnified image. The EDS analysis results corresponding to points 1, 2, and 3 are presented in Table 3.

Table 3. EDS analysis results for the different selected areas in Fig. 5(b) at%

Points	Ti	C	Al	O	Si
1	25.88	—	67.89	—	6.23
2	64.11	35.89	—	—	—
3	—	—	50.59	49.41	—

4.2. Analysis of the phase and microstructure of the specimen heated at 1773 K

Fig. 6 shows the XRD patterns of T0-1773 and T1-1773. No Al_4O_4C or Al_4C_3 was detected in T1-1773, and the diffraction peak intensities of the TiC alloy and Al_3Ti are substantially larger and smaller, respectively, than those of T1-1573. Meanwhile, with an increase in the firing temperature from 1573 to 1773 K, the diffraction peak position of the TiC crystal was shifted to a large angle, demonstrating that the TiC crystal was converted into a TiCN crystal [33] (Fig. 7). A new phase, $(Al_2OC)_x(AlN)_{1-x}$, was formed in T0-1773.

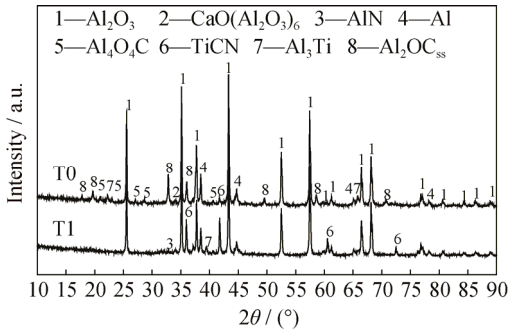

Fig. 6. XRD patterns of the specimens T0 and T1 after being sintered at 1773 K for 3 h.

SEM images of T0-1773 and T1-1773 are presented in Figs. 8 and 9, respectively. Fig. 8 shows that the structure of T0-1773 is still loose, fine particles and that regular circular holes left by metal Al still exist. By contrast, Fig. 9(a) shows that the T1-1573 exhibited good sintering properties; TiCN and Al_2O_3 particles in the matrix were tightly bonded together. The results of the EDS analysis (Table 4) of bright-white particles in Fig. 9(b) show that the TiCN particle indeed contains N.

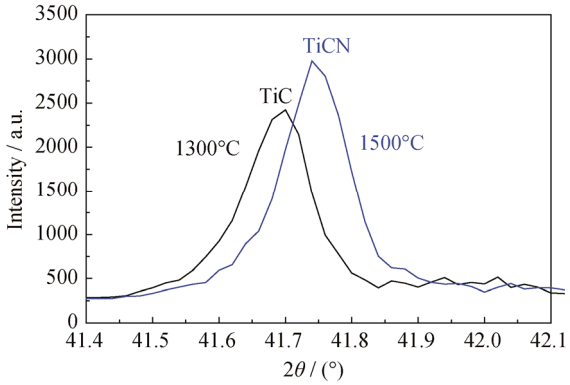

Fig. 7. Diffraction peak corresponding to the TiC crystal in the XRD patterns of T1 heated at 1573 and 1773 K.

4.3. Phase evolution process analysis

Under the conditions of low oxygen partial pressure, TiO_2 itself will deoxidize to form suboxides. The reaction equations are as follows:

$$6\,TiO_2(s) = 2\,Ti_3O_5(s) + O_2(g) \quad (8)$$

$$4\,Ti_3O_5(s) = 6\,Ti_2O_3(s) + O_2(g) \quad (9)$$

$$2\,Ti_2O_3(s) = 4\,TiO(s) + O_2(g) \quad (10)$$

$$2\,TiO(s) = 2\,Ti(s) + O_2(g) \quad (11)$$

The stability of titanium oxides in the temperature range 1000–2000 K is shown in the plot of $\lg(\frac{P_{O_2}}{P^{\ominus}})$ vs. T in Fig. 10. Under the condition of a low oxygen partial pressure caused by the reaction $2\,C(s) + O_2(g) = 2\,CO(g)$ (oxygen partial pressure is given by $\lg(\frac{P_{O_2}}{P^{\ominus}}) = -14.55 - \frac{11672.19}{T}$), TiO_2 will gradually decompose according to the process $TiO_2 \rightarrow Ti_3O_5 \rightarrow Ti_2O_3$ as the firing temperature increases. Under this condition, the formation process of Al_3Ti in the material can be expressed as

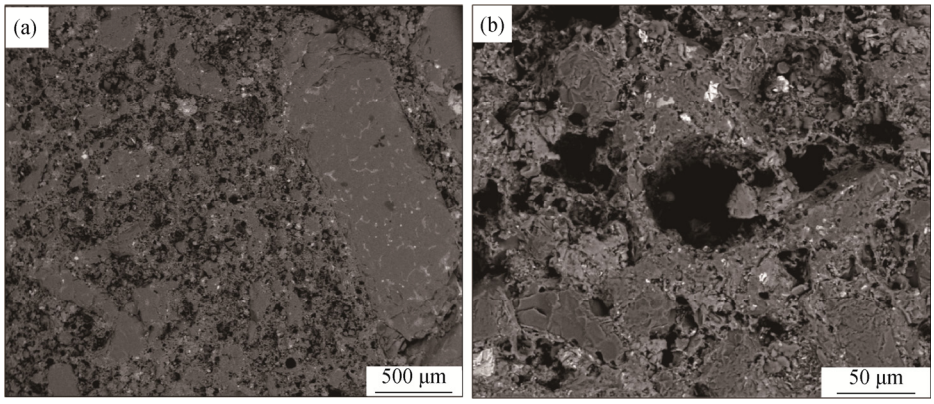

Fig. 8. SEM image of sample T0-1773: (a) macro image; (b) partially magnified image.

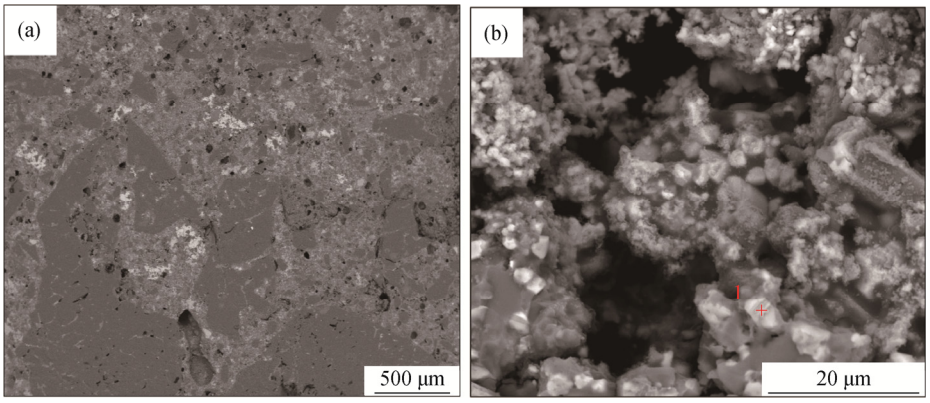

Fig. 9. SEM images of sample T1-1773: (a) macro image; (b) partially magnified image.

Table 4. EDS analysis results for the bright-white particles in Fig. 9(b) at%

Ti	Al	C	N	O
49.39	1.8	31.62	10.93	6.26

$$4\,Al(l) + 3\,TiO_2(s) = 3\,Ti(s) + 2\,Al_2O_3(s) \quad (12)$$

$$10\,Al(l) + 3\,Ti_3O_5(s) = 9\,Ti(s) + 5\,Al_2O_3(s) \quad (13)$$

$$2\,Al(l) + Ti_2O_3(s) = 2\,Ti(s) + Al_2O_3(s) \quad (14)$$

$$3\,Al(l) + Ti(s) = Al_3Ti(s) \quad (15)$$

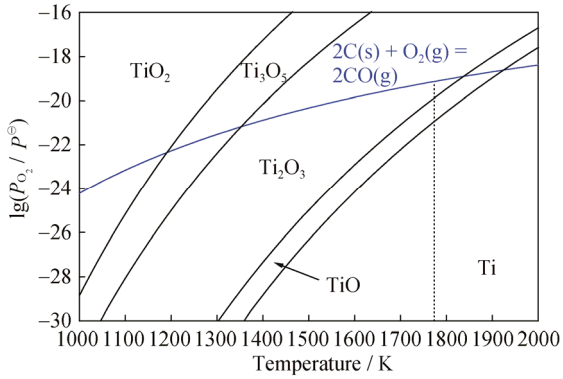

Fig. 10. Stability of titanium oxide in the temperature range of 1000–2000 K, as shown in a plot of $\lg(\frac{P_{O_2}}{P^{\ominus}})$ as a function of *T*.

The Al–Ti binary phase diagram (Fig. 1) shows that, when the firing temperature is raised to 1773 K, Al_3Ti is converted into liquid Al–Ti alloy. The activity of Ti in Al–Ti alloy was calculated by Kostov *et al*. [34]; their results are shown in Table 5. The data in Table 5 were fitted using the Origin software; the relationship between the activity of Ti (a_{Ti}) and the composition of Al–Ti alloy is shown in Eq. (16):

$$a_{Ti} = 3.515\times10^{-4} + 0.3052X_{Ti} - 2.052X_{Ti}^2 + 6.963X_{Ti}^3 - 4.222X_{Ti}^4 \quad (16)$$

The partial pressure of Ti(g) in the Al–Ti alloy is given by $P_{Ti} = P_{Ti}^* \times a_{Ti}$, where P_{Ti}^* is the saturated vapor pressure of pure titanium ($\lg\left(\frac{P_{Ti}^*}{P^{\ominus}}\right) = \frac{-23472.08}{T} + 5.53$). Under the condition of a low oxygen partial pressure caused by the reaction of C(s) and O_2(g), the relationship between the partial pressure of Ti(g) and the composition of Al–Ti alloy is expressed as

Table 5. Activity of Ti in Al–Ti alloy at 1773 K [34]

X_{Ti}	0	0.1	0.2	0.3	0.4	0.5	0.6	0.7	0.8	0.9	1
a_{Ti}	0	0.015141	0.032151	0.064489	0.12757	0.23813	0.40118	0.59423	0.77232	0.90274	1

$$\lg\left(\frac{P_{Ti}}{P^{\ominus}}\right) = -7.7 + 0.434\ln(3.515\times10^{-4} + 0.3052X_{Ti} - 2.052X_{Ti}^2 + 6.963X_{Ti}^3 - 4.222X_{Ti}^4) \quad (17)$$

When O_2(g) is present in the system, Ti(g) can be converted into TiO(g) and TiO_2(g):

$$Ti(g) + 0.5O_2(g) = TiO(g) \quad (18)$$

$$Ti(g) + O_2(g) = TiO_2(g) \quad (19)$$

The relationship between the gas partial pressures of Ti(g), TiO(g), and TiO_2(g) and the Al–Ti alloy composition was plotted; the results are shown in Fig. 11. The gas-phase mass transfer of elemental Ti in the material is mainly carried out in the form of Ti(g) and TiO(g). The formation of fibers on the surface of TiCN particles in sample T1-1773 indicated the gas-phase mass transfer of Ti (Fig. 12).

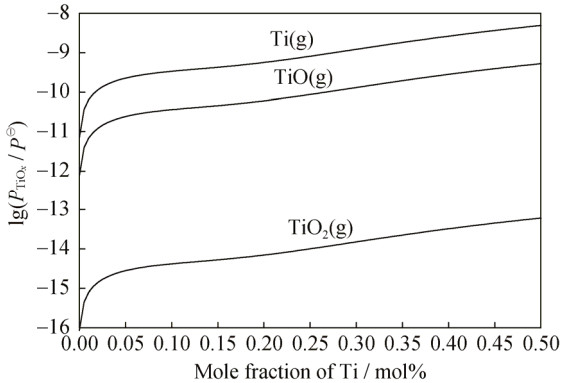

Fig. 11. Relationship of gas partial pressure of Ti(g), TiO(g), and TiO_2(g) with Ti content in Al–Ti alloy.

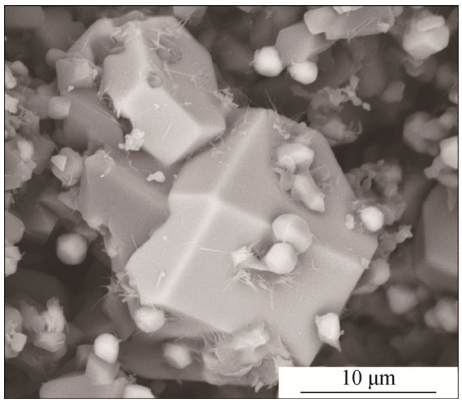

Fig. 12. Fibrous forms on the surface of TiCN particles in sample T1-1773.

The cubic TiC exhibits deviations in stoichiometry over a wide range of homogeneity, from $TiC_{0.47}$ to TiC_1, as a result of vacancies in the carbon sublattice. As the vacancy concentration in the TiC_x crystal increases, the structure of TiC_x does not change [35] and the lattice constant becomes smaller [36]. The XRD results show that the lattice constant of TiC_x generated in T1-1573 is 0.4327 nm, which is less than that of stoichiometric TiC (0.4329 nm). The C vacancies in the TiC_x crystal structure provide a channel for the diffusion of N at high temperatures; the formation of TiCN in the material can be expressed as

$$Ti(g)/TiO(g) + N_2(g) + TiC_x(s) \rightarrow TiCN(s) \quad (20)$$

On the basis of the aforementioned results and analyses,

the phase transformation process of the Al–TiO_2–Al_2O_3 composite at high temperatures under flowing N_2 is explained as follows: After the specimen is heated to 853 K and held for 8 h under flowing N_2, the thermosetting phenolic resin is converted into carbon and the Al metal reacts with N_2 to form an Al–AlN core–shell structure. As the firing temperature increases, the molten Al loses the protection of the AlN shell and flows through the pores of the material. Because of the strong reducibility of the metal Al, TiO_2 is reduced to Al_3Ti alloy and then Al_3Ti reacts with C and other carbides (Al_4C_3 and Al_4O_4C) to form TiC_x ($x < 1$); Ti(g) and TiO(g) are produced after Al_3Ti is converted into a liquid phase. Under N_2 conditions, Ti(g) and TiO(g) are further nitrided and solid-dissolved into the TiC_x crystal to form a TiCN solid solution.

Both Al_2O_3 and TiCN are rigid compounds, and the formation of these rigid particles in the alloy phase reduces the flowability and prevents the composition of the material from becoming uneven at high temperatures. A special structure of plastic alloy that toughens the rigid composite and rigid particle-reinforced plastic alloy is formed in the material. The phase and microstructure evolution of Al–Al_2O_3 and Al–TiO_2–Al_2O_3 composites during the firing process are shown in Fig. 13.

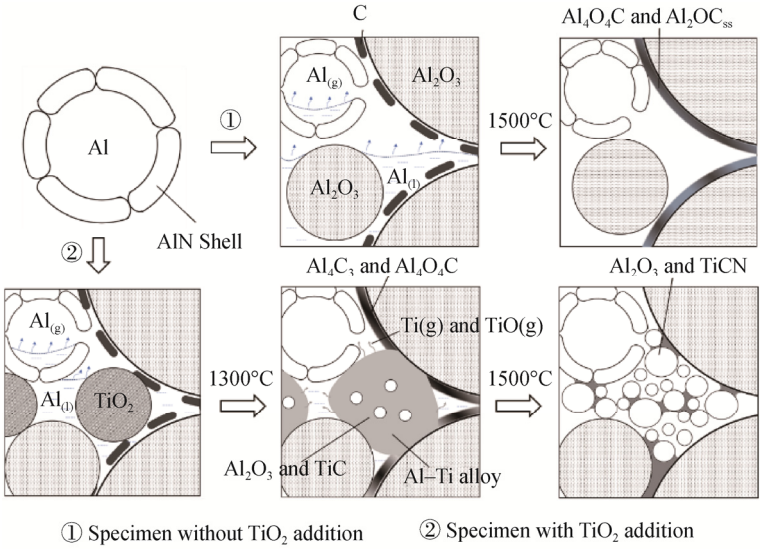

Fig. 13. Phase and microstructure evolution of Al–Al_2O_3 and Al–TiO_2–Al_2O_3 composites during the firing process.

5. Conclusions

The metal Al exhibits good fluidity at high temperatures, which is detrimental to the performance of Al-containing refractories. In this study, TiO_2 was used to consume the Al generated in the Al–Al_2O_3 composite under high-temperature and N_2 conditions. The phase and microstructure of the Al–TiO_2–Al_2O_3 composites after sintering were studied. The results are summarized as follows:

(1) During the firing of the Al–TiO_2–Al_2O_3 composite, TiO_2 can absorb the metal Al fluid and transform it into a high-temperature plastic phase, Al_3Ti, which causes the structure of the material to rearrange, enhancing the compactness of the material. The microstructure of the Al–TiO_2–Al_2O_3 composite after sintering at 1773 K for 3 h under N_2 is dense; by contrast, the Al–Al_2O_3 composite exhibits a loose structure.

(2) A novelty phase, TiCN, is produced in the fired Al–TiO_2–Al_2O_3 composite at 1773 K under flowing N_2. The mechanism of formation of the TiCN is explained as follows: TiO_2 reacts with Al to form Al_3Ti alloy. The Al_3Ti then reacts with C and other carbides (Al_4C_3 and Al_4O_4C) to form TiC_x, whereas Ti(g) and TiO(g) are produced after Al_3Ti is converted into a liquid phase. Under N_2 conditions, Ti(g) and TiO(g) are further nitrided and solid-dissolved into the TiC_x crystals to form a TiCN solid solution.

Acknowledgements

Authors acknowledge the financial support from the National Natural Science Foundation of China (No. 51872023).

References

[1] E.M.M. Ewais, Carbon based refractories, *J. Ceram. Soc. Jpn.*, 112(2004), No. 1310, p. 517.

[2] T.B. Zhu, Y.W. Li, S.B. Sang, and Z.P. Xie, Improved thermal shock resistance of magnesia-graphite refractories by the

addition of MgO–C pellets, *Mater. Des.*, 124(2017), p. 16.

[3] W. Yang, X.H Wang, L.F. Zhang, Q.L. Shan, and X.F. Liu, Cleanliness of low carbon aluminum-killed steels during secondary refining processes, *Steel Res. Int.*, 84(2013), No. 5, p. 473.

[4] C.H. Ma, Y. Li, M.W. Yan, Y. Sun, and J.L. Sun, Investigation on a postmortem resin-bonded Al-Si-Al_2O_3, sliding gate with functional gradient feature, *Ceram. Int.*, 44(2018), No. 6, p. 6384.

[5] C. Atzenhofer, S. Gschiel, and H. Harmuth, Phase formation in Al_2O_3–C refractories with Al addition, *J. Eur. Ceram. Soc.*, 37(2016), No. 4, p. 1805.

[6] P. Jiang, J.L. Sun, W.D. Xue, J.H. Chen, R.V. Kumar, and Y. Li, New synthetic route to Al_4O_4C reinforced Al–Al_2O_3 composite materials, *Solid State Sci.*, 46(2015), p. 33.

[7] M.W. Yan, Y. Li, H.Y. Li, and J.L. Sun, Theoretical analysis and synthesis of Al_4O_4C and Al_2CO phase in the resin bonded Al–Al_2O_3 refractory in N_2-flowing, *Ceram. Int.*, 44(2017), No. 2, p. 1493.

[8] S. Zhang and A. Yamaguchi, Hydration resistances and reactions with CO of Al_4O_4C and Al_2OC formed in carbon-containing refractories with Al, *J. Ceram. Soc. Jpn.*, 104(1996), No. 1209, p. 393.

[9] C.A. Qiu and R. Metselaar, Thermodynamic evaluation of the Al_2O_3–Al_4C_3 system and stability of Al-oxycarbides, *Z. Metallkd.*, 86(1995), No. 3, p. 198.

[10] E.L. Amma and G.A. Jeffrey, Structure of aluminum oxycarbide Al_2OC: a short-range wurtzite super-structure, *J. Chem. Phys.*, 34(1961), No. 1, p. 252.

[11] J.M. Lihrmann, J. Tirlocq, P. Descamps, and F. Cambier, Thermodynamics of the Al–C–O system and properties of SiC–AlN–Al_2OC composites, *J. Eur. Ceram. Soc.*, 19(1999), No. 16, p. 2781.

[12] J.M. Lihrmann, Thermodynamics of the Al_2O_3–Al_4C_3 system: I. Thermochemical functions of Al oxide, carbide and oxycarbides between 298 and 2100 K, *J. Eur. Ceram. Soc.*, 28(2008), No. 3, p. 633.

[13] J.M. Lihrmann, Thermodynamics of the Al_2O_3–Al_4C_3 system: II. Free energies of mixing, solid solubilities and activities, *J. Eur. Ceram. Soc.*, 28(2008), No. 3, p. 643.

[14] J.M. Lihrmanm, Thermodynamics of the Al_2O_3-Al_4C_3 system: III. Equilibrium vapour pressures and activation energies for volatilization, *J. Eur. Ceram. Soc.*, 28(2008), No. 3, p. 649.

[15] J.M. Lihrmann, T. Zambetakis, and M. Daire, High-temperature behavior of the aluminum oxycarbide Al_2OC in the system Al_2O_3–Al_4C_3 and with additions of aluminum nitride, *J. Am. Ceram. Soc.*, 72(1989), No. 9, p. 1704.

[16] S.Y. Kuo and A.V. Virkar, Phase equilibria and phase transformation in the aluminum nitride–aluminum oxycarbide pseudobinary system, *J. Am. Ceram. Soc.*, 72(1989), No. 4, p. 540.

[17] K. Motzfeldt, Comment on "Thermodynamics of the Al–C–O ternary system" [J. Electrochem. Soc. 153, E119 (2006)], *J. Electrochem. Soc.*, 154(2007), No. 3, p. S1.

[18] K. Cheng, C. Yu, J. Ding, C.J. Deng, H.X. Zhu, and Z.L. Xue, Synthesis and characterization of AlN whiskers by nitridation of Al_4O_4C, *J. Alloys Compd.*, 719(2017), p. 308.

[19] K. Cheng, C.J. Deng, J. Ding, C. Yu, and H.X. Zhu, Synthesis of Al_2O_3 nanowires by heat-treating Al_4O_4C in a carbon-containing environment, *Ceram. Int.*, 44(2017), No. 5, p. 4996.

[20] Y.B. Li, Y. Bando, and D. Golberg, Single-crystalline α-Al_2O_3 nanotubes converted from Al_4O_4C nanowires, *Adv. Mater.*, 17(2005), No. 11, p. 1401.

[21] H.G. Zhu, Y.L. Jiang, Y.Q. Yao, J.Z. Song, J.L. Li, and Z.H. Xie, Reaction pathways, activation energies and mechanical properties of hybrid composites synthesized in-situ from Al–TiO_2–C powder mixtures, *Mater. Chem. Phys.*, 137(2012), No. 2, p. 532.

[22] T.D. Xia, T.Z. Liu, W.J. Zhao, B.Y. Ma, and T.M. Wang, Self-propagating high-temperature synthesis of Al_2O_3–TiC–Al composites by aluminothermic reactions, *J. Mater. Sci.*, 36(2001), No. 23, p. 5581.

[23] Y.M.Z. Ahmed, Z.I. Zaki, D.H.A. Besisa, A.M.M Amin, and R.K. Bordia, Effect of zirconia and iron on the mechanical properties of Al_2O_3/TiC composites processed using combined self-propagating synthesis and direct consolidation technique, *Mater. Sci. Eng. A*, 696(2017), p. 182.

[24] A. Hajalilou, M. Hashim, M. Nahavandi, and I. Ismail, Mechanochemical carboaluminothermic reduction of rutile to produce TiC–Al_2O_3, nanocomposite, *Adv. Powder Technol.*, 25(2014), No. 1, p. 423.

[25] R. Yamanoglu, N. Gulsoy, E.A. Olevsky, and H.O. Gulsoy, Production of porous $Ti_5Al_{2.5}Fe$ alloy via pressureless spark plasma sintering, *J. Alloys Compd.*, 680(2016), p. 654.

[26] A. Rajabi, M.J. Ghazali, and A.R. Daud, Chemical composition, microstructure and sintering temperature modifications on mechanical properties of TiC-based cermet–A review, *Mater. Des.*, 67(2015), p. 95.

[27] M.W. Yan, Y. Li, J.J. Wang, H.Y. Li, Y. Sun, and C.H. Ma. Phase evolution mechanism of non-oxide bonded Al–Al_2O_3–MgO–ZrO_2 composites at 1873K in flowing nitrogen, *J. Am. Ceram. Soc.*, 101(2017), No. 5, p. 2162.

[28] U.R. Kattner, J.C. Lin, and Y.A Chang, Thermodynamic assessment and calculation of the Ti–Al system, *Metall. Trans. A*, 23(1992), No. 8, p. 2081.

[29] M. Mirjalili, M. Soltanieh, K. Matsuura, and M. Ohno, On the kinetics of $TiAl_3$ intermetallic layer formation in the titanium and aluminum diffusion couple, *Intermetallics.*, 32(2013), p. 297.

[30] M. Sujata, S. Bhargava, and S. Sangal. On the formation of $TiAl_3$ during reaction between solid Ti and liquid Al, *J. Mater. Sci. Lett.*, 16(1997), No. 13, p. 1175.

[31] M.Z. Mehrizi, R. Beygi, and G. Eisaabadi, Synthesis of Al/TiC–Al_2O_3 nanocomposite by mechanical alloying and subsequent heat treatment, *Ceram. Int.*, 42(2016), No. 7, p. 8895.

[32] M.W. Chase Jr, *NIST-JANAF Thermochemical Tables,* 4th ed., American Chemical Society and the American Institute of Physics for the National Institute of Standards and Technology, Washington DC, 1998.

[33] Y.F. Qin, G.F. Zheng, L.Y. Zhu, J.N. He, F.Y. Zhang, Y.C. Dong, and F.C. Yin, Structure and wear characteristics of TiCN nanocomposite coatings fabricated by reactive plasma spraying, *Surf. Coat. Technol.*, 342(2018), p. 137.

[34] A. Kostov, B. Friedrich, and D. Zivkovic, Predicting thermodynamic properties in Ti–Al binary system by FactSage, *Comput. Mater. Sci.*, 37(2006), No. 3, p. 355.

[35] N.J. Ashley, R.W. Grimes, and K.J. McClellan, Accommodation of non-stoichiometry in TiN_{1-x}, and ZrN_{1-x}, *J. Mater. Sci.*, 42(2007), No. 6, p. 1884.

[36] Z. Dridi, B. Bouhafs, P. Ruterana, and H. Aourag, First-principles calculations of vacancy effects on structural and electronic properties of TiC_x and TiN_x, *J. Phys. Condens. Matter*, 14(2002), No. 43, p. 10237.